# Coherent spectroscopy with a single antiproton spin

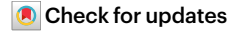
https://doi.org/10.1038/s41586-025-09323-1

Received: 10 March 2025

Accepted: 23 June 2025

Published online: 23 July 2025

Open access



B. M. Latacz<sup>1,2</sup>, S. R. Erlewein<sup>1,3,4</sup>, M. Fleck<sup>2,5</sup>, J. I. Jäger<sup>1,4</sup>, F. Abbass<sup>3</sup>, B. P. Arndt<sup>4,6</sup>, P. Geissler<sup>2</sup>, T. Imamura<sup>7,8</sup>, M. Leonhardt<sup>3</sup>, P. Micke<sup>1,4</sup>, A. Mooser<sup>4</sup>, D. Schweitzer<sup>3</sup>, F. Voelksen<sup>3</sup>, E. Wursten<sup>2</sup>, H. Yildiz<sup>9</sup>, K. Blaum<sup>4</sup>, J. A. Devlin<sup>1,10</sup>, Y. Matsuda<sup>5</sup>, C. Ospelkaus<sup>7,8</sup>, W. Quint<sup>6</sup>, A. Soter<sup>11</sup>, J. Walz<sup>9,12</sup>, Y. Yamazaki<sup>2</sup>, C. Smorra<sup>3</sup> & S. Ulmer<sup>2,3</sup> ≅

Coherent quantum transition spectroscopy is a powerful tool in metrology<sup>1</sup>, quantum information processing<sup>2</sup>, magnetometry<sup>3</sup> and precision tests of the standard model<sup>4</sup>. It was applied with great success in proton and deuteron magnetic moment measurements<sup>5</sup>, which culminated in maser spectroscopy with sub-parts-per-trillion resolution<sup>6</sup> and many other experiments at the forefront of physics<sup>7</sup>. All of these experiments were performed on macroscopic ensembles of particles, whereas the coherent spectroscopy of a 'free' single nuclear spin has, to our knowledge, never been reported before. Here we demonstrate coherent quantum transition spectroscopy of the spin of a single antiproton stored in a cryogenic Penning-trap system. We apply a multi-trap technique<sup>8</sup>, detect the antiproton spin state using the continuous Stern-Gerlach effect<sup>9</sup> and transport the particle to the homogeneous magnetic field of a precision trap (PT). Here we induce the coherent dynamics and analyse the result by quantum-projection measurements in the analysis trap (AT)<sup>10</sup>. We observe, for the first time, Rabi oscillations of an antiproton spin and achieve in time-series measurements spin-inversion probabilities greater than 80% at spin coherence times of about 50 s. Scans of single-particle spin resonances show inversions greater than 70%, at transition linewidths 16 times narrower than in previous measurements<sup>8</sup>, limited by cyclotron frequency measurement decoherence. This achievement marks a notable step towards at least tenfold improved tests of matter/antimatter symmetry using proton and antiproton magnetic moments.

Precision measurements of the magnetic properties of simple systems stand as a powerful tool for investigating fundamental physics, enabling some of the most precise tests of symmetry violations. For instance, the experiments described in ref. 11 used a 3He/129Xe comagnetometer to place tight constraints on CPT-invariance-violating and Lorentzinvariance-violating parameters for neutrons<sup>12</sup>. Incoherent studies of the magnetic properties of single electrons<sup>13</sup> provide unparalleled tests of the Standard Model, while also setting constraints on the parameter space in which the dark photon could exist<sup>14</sup>. Meanwhile, direct measurements on <sup>3</sup>He<sup>+</sup> and <sup>9</sup>Be<sup>+</sup> ions have established the most precise absolute magnetometers so far<sup>15</sup> and test multi-electron shielding factors<sup>16</sup>. Our experiments focus on antimatter-based magnetometry<sup>17</sup> using cryogenic multi-Penning-trap systems. We have measured the proton (p) magnetic moment with a fractional accuracy of 300 ppt (ref. 18) and determined that of the antiproton  $(\overline{p})$  with 1.5 ppb resolution<sup>8</sup>. These experiments are based on incoherent spin-projection measurements using the continuous Stern-Gerlach effect 19,20, combined with decoherent measurements of the Larmor  $v_L$  and the cyclotron  $v_c$  frequencies in the magnetic field  $B_0 = 1.945$  T of our PT (ref. 21). The ratio of the measured frequencies gives the gyromagnetic g-factor  $g/2 = \nu_{\rm l}/\nu_{\rm c}$ . Decoherent Larmor resonance spectroscopy results in suppressed spin inversion and contributes to the broadening of the measured resonance lines, both of which diminish measurement resolution. Establishing coherent techniques to overcome these limitations is an exciting prospect and represents a key advancement towards establishing nuclear magnetic moment measurements at substantially improved resolution.

Here we demonstrate the coherent quantum transition spectroscopy of a single nuclear spin 1/2 particle—a single trapped antiproton. The measurements are carried out in the multi-Penning-trap system of the BASE collaboration at the Antiproton Decelerator (AD)/ELENA facility of CERN. By applying our unique two-particles/three-traps technique, supported by our cooling trap (CT)<sup>22</sup>, we observe Rabi oscillations of a single  $\overline{p}$  spin and achieve spin coherence times greater than 50 s. In line-shape scans, in which we vary an applied spin-flip radiofrequency  $v_{\rm rf}$  with respect to the Larmor frequency  $v_{\rm L} = \left(\frac{g_p}{2}\right) \times v_{\rm c}$ , we obtain spin inversions greater than 70% and a full width at half maximum (FWHM) of the spin-transition resonance that is below

<sup>1</sup>CERN, Geneva, Switzerland. <sup>2</sup>Ulmer Fundamental Symmetries Laboratory, RIKEN, Wako, Japan. <sup>3</sup>Lehrstuhl für Quantentechnologie und Fundamentalphysik, Heinrich-Heine-Universität Düsseldorf, Düsseldorf, Germany. <sup>4</sup>Max-Planck-Institut für Kernphysik, Heidelberg, Germany. <sup>5</sup>Graduate School of Arts and Sciences, University of Tokyo, Meguro, Japan. <sup>6</sup>GSI Helmholtzzentrum für Schwerionenforschung GmbH, Darmstadt, Germany. <sup>7</sup>Institut für Quantenoptik, Leibniz Universität Hannover, Hanover, Germany. <sup>8</sup>Physikalisch-Technische Bundesanstalt, Braunschweig, Germany. <sup>9</sup>Institut für Physik, Johannes Gutenberg-Universität Mainz, Mainz, Germany. <sup>10</sup>Center for Cold Matter, Blackett Laboratory, Imperial College London, London, UK. <sup>11</sup>ETH Zürich, Zürich, Switzerland. <sup>12</sup>Helmholtz-Institut Mainz, Johannes Gutenberg-Universität Mainz, Mainz, Germany. <sup>58</sup>e-mail: stefan.ulmer@cern.ch

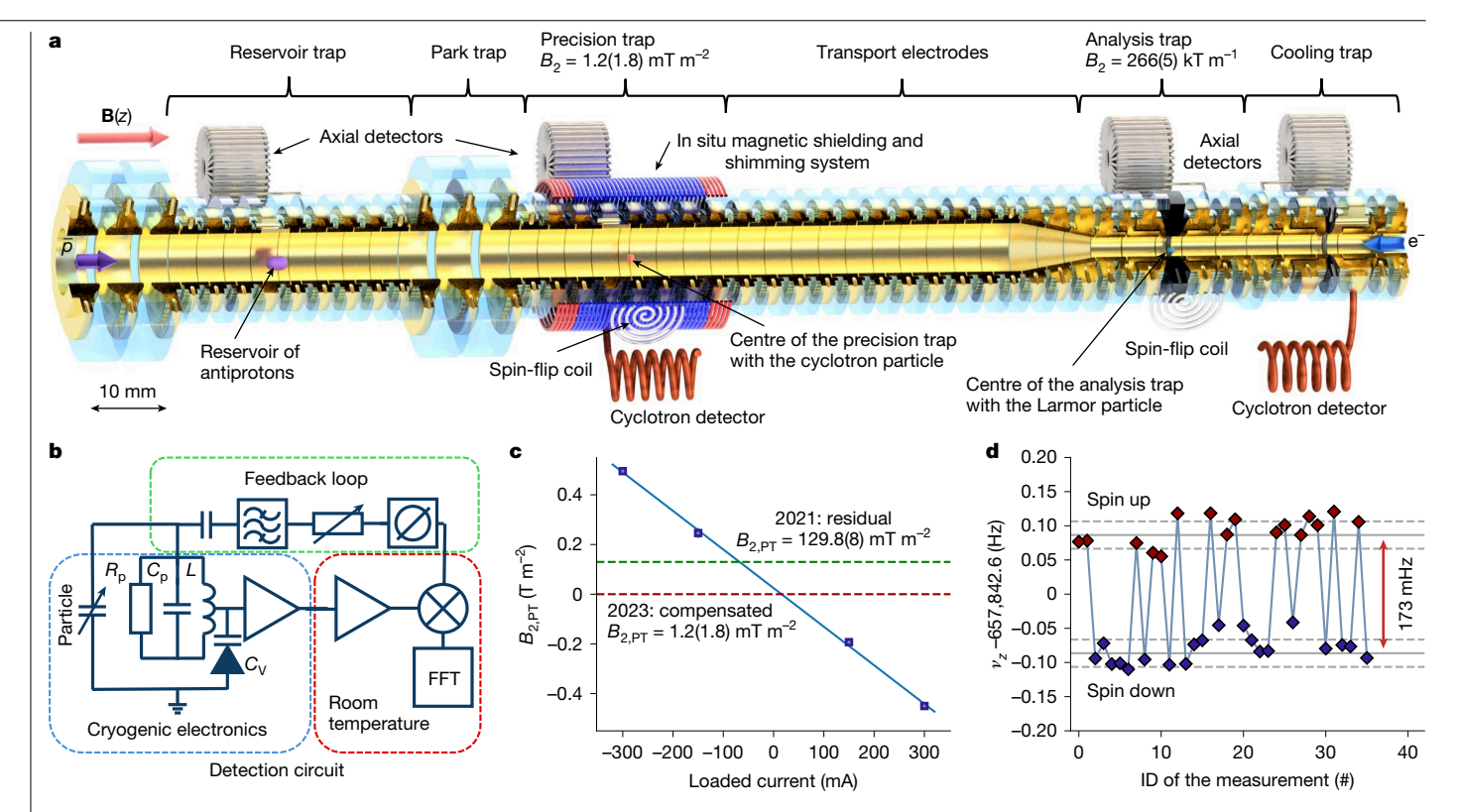


Fig. 1 | Experimental set-up. a, Multi-Penning trap to demonstrate coherent spin quantum transitions with a single trapped antiproton. The trap stack consists of an antiproton reservoir trap, a park trap, a highly homogeneous and shielded precision trap, an analysis trap to apply the continuous Stern-Gerlach effect and a trap to cool the antiproton's modified cyclotron mode. The trap electrodes (golden) are spaced by sapphire rings (blue shading). b, Schematic of a single-particle detection system. The detector is represented by a parallel

RLC circuit, with inductance  $L \approx 2$  mH, capacitance  $C_p \approx 25$  pF and  $R_p \approx 150$  M $\Omega$ . c, Magnetic bottle strength in the centre of the precision trap, as a function of current applied to the persistent local superconducting magnet. Error bars are smaller than the size of the data points. d, Non-destructive detection of spin transitions in the centre of the analysis trap by measuring the axial frequency of the single trapped antiproton. Each frequency measurement takes around 120 s.

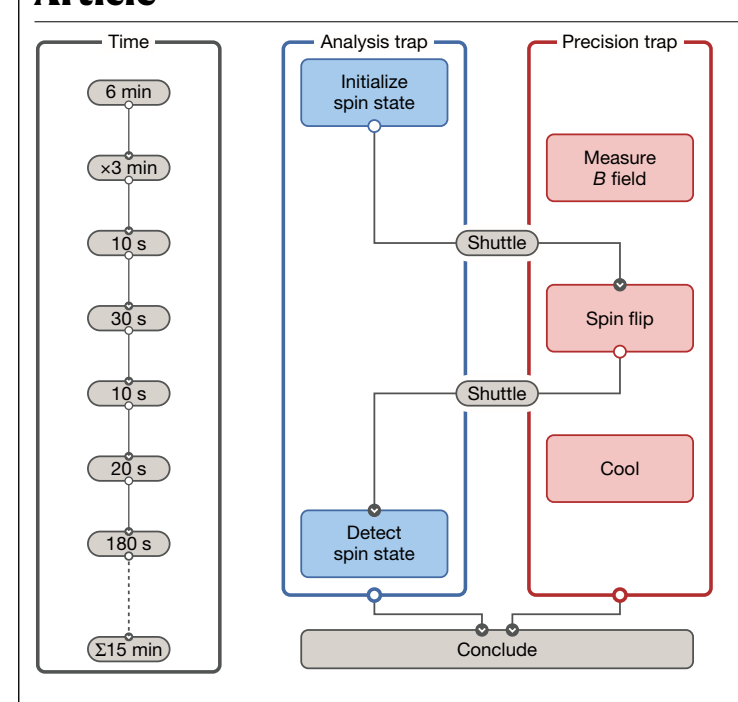
200 mHz. This is more than ten times narrower than in our previous antiproton magnetic moment measurements<sup>8</sup>. We show that the FWHM is, at present, limited by decoherence induced by cyclotron frequency measurement noise. This is a crucial step towards improved measurements of the p and  $\overline{p}$  magnetic moments with a fractional accuracy less than 100 ppt and will allow for searches of time signatures of asymmetric antimatter/dark matter coupling<sup>23</sup> at improved mass resolution and increased data-taking rate, thanks to the higher signal-to-noise ratio and smaller FWHM of the coherent measurements.

The heart of our experiment is a superconducting solenoid magnet with a horizontal bore, operated at a magnetic field of  $B_{0,PT}$  = 1.945 T. Inside the bore, the cryogenic multi-Penning-trap system, shown in Fig. 1, is mounted. Most important for this study are the AT, in which the continuous Stern-Gerlach effect is applied<sup>19</sup>, the homogeneous PT, in which precision frequency measurements take place, and a park trap (PKT). AT and PT centres are separated by 73.4 mm and PT and PKT centres are separated by 18.6 mm. The trap stack is placed inside a cylindrical hermetically sealed, pinched, cryo-pumped vacuum chamber, in which pressures less than  $10^{-18}$  mbar and (anti)particle storage times of years are achieved<sup>24</sup>. The trap electrodes, designed as in ref. 25, are primarily made out of gold-plated copper. The central ring electrode of the AT is made of ferromagnetic CoFe, also gold-plated, which distorts the magnetic field in the centre of the trap to  $B_{AT}(z) = B_{0,AT} + B_{2,AT} \times$  $(z - z_{AT,0})^2$ , in which  $B_{0,AT} = 1.231$  T,  $B_{2,AT} = 266(5)$  kT m<sup>-2</sup> and  $z_{AT,0}$  is the trap centre (Fig. 1a). The magnetic field in the centre of the PT is  $B_{\rm PT}(z)$  =  $B_{0,\text{PT}} + B_{1,\text{PT}} \times (z - z_{\text{PT},0}) + B_{2,\text{PT}} \times (z - z_{\text{PT},0})^2$ , with  $z_{\text{PT},0}$  being the centre of the trap. Achieved with a local persistent magnet system, the coefficient  $B_{2,\rm PT}$  can be tuned in a range of about  $\pm 350$  mT m<sup>-2</sup>. The gradient field  $B_{1,PT}$  can be adjusted in a range between 10 mT m<sup>-1</sup> and 24 mT m<sup>-1</sup>.

Also part of the magnet system is a set of self-shielding solenoids<sup>26,27</sup>, with a shielding factor greater than 50. The trap electrodes are biased with ultrastable voltage sources. The applied voltages are selected such that, in the trap centres, homogeneous quadrupolar potentials  $\Phi(z, \rho) = V_0 C_2(z^2 - \rho^2/2)$  are formed<sup>25</sup>. Here  $V_0$  is the voltage applied to the central ring electrode,  $C_2$  is a geometry coefficient (Extended Data Table 1 and Methods) and z and  $\rho$  are cylindrical coordinates, for which z points along the magnetic field axis. A single particle in such crossed static fields oscillates at three independent frequencies<sup>28</sup>, at the modified cyclotron frequency  $v_{+,PT} \approx 29.645$  MHz, the axial frequency  $v_{z,PT} \approx 637 \text{ kHz}$  and the magnetron frequency  $v_{-,PT} \approx 7 \text{ kHz}$ . An invariance theorem  $v_c^2 = v_+^2 + v_z^2 + v_-^2$  (ref. 28) relates the free cyclotron frequency  $v_c = (qB_0)/(2\pi m)$  to  $v_+$ ,  $v_z$  and  $v_-$ ; here q and m are the charge and the mass of the single trapped particle, respectively. Details on the eigenfrequencies and their measurements using non-destructive detection (see Fig. 1b) are described in Methods and summarized in Extended Data Tables 1 and 2.

To implement the coherent spin transition spectroscopy, we use the two-particles/three-traps technique described in ref. 8. The measurement protocol is shown in Fig. 2. First, we initialize the spin state of a cold 'Larmor' particle in the AT. A second antiproton, the 'cyclotron' particle, is prepared in the PT for high-precision  $v_{c,PT}$  measurements to determine the magnetic field of the trap<sup>29</sup>. After initialization, the Larmor particle is transported to the PT, at which a spin-flip drive is applied. The particle is then returned to the AT to determine whether a spin transition has occurred.

To begin, we first use the magnetic shimming system (Fig. 1a,c) and use measurements with the cyclotron particle to tune the magnetic coefficient  $B_{2,PT}$ . In the case of finite  $B_{2,PT}$ , interaction of the



 $\textbf{Fig. 2} \ | \ \textbf{Measurement protocol.} \ Illustration of the experiment sequence described in the text.$ 

particle with the axial detector causes axial rms-amplitude fluctuations  $\propto (k_{\rm B}T_z/m\omega_z^2)$ . These shift the Larmor frequency by  $\Delta v_{\rm L} = (1/4\pi^2) \, (v_{\rm L}/v_z^2) \, (B_2/B_0) \, (k_{\rm B}T_z/m)$  with the particle-to-detector correlation time of about 100 ms, causing motional spin decoherence. We thus tune  $B_{2,\rm PT} = 1.2 \, (1.8) \, \rm mT \, m^{-2}$ , corresponding at the temperature  $T_{z,\rm PT} = 8.5 \, (3) \, \rm K$  of the PT axial detector to spin coherence times longer than 1 h (ref. 28). Next, we apply the cooling protocol described in ref. 22 to the Larmor particle and cool it to a cyclotron energy  $E_+/k_{\rm B} = T_+ < 100 \, \rm mK$ . Owing to the presence of the strong magnetic bottle  $B_{2,\rm AT}$ , a spin transition induces an axial frequency shift of  $\Delta v_{z,\rm SF} = 173 \, (1) \, \rm mHz$  (ref. 19). A sequence of axial frequency measurements  $v_{z,\rm AT}$  interleaved by spin transitions is shown in Fig. 1d.

To initialize the spin state of the Larmor particle, we apply a sequence of  $v_{z,AT}$  measurements, each taking 120 s, followed by a 10 s injection of a magnetic spin-flip drive at  $v_{rf,AT}$  = 51.651 MHz. At the background  $v_{z,AT}$ scatter<sup>10</sup>  $\Xi_{\text{back},AT} \approx 32(2)$  mHz achieved in this trap, we identify a measured  $v_{z,AT}$  difference  $\Delta v_{z,SF} > 140$  mHz as a spin transition. This leads to spin-state initialization with a confidence of about 100%. Subsequently, we use the cyclotron particle in the PT to determine  $B_{0,PT}$  in this trap. To that end, we measure  $v_{c,PT}$ , using the technique described in ref. 29. A single cyclotron frequency measurement of approximately 180 s resolves  $v_c$  with a fractional uncertainty of  $\sigma(v_{c,PT})/v_{c,PT} = 1.42(7)$  ppb. This frequency defines the radiofrequency that is irradiated to later induce the coherent spin transitions in the PT  $v_{rf,SF,PT} = (g_p/2) \times v_{c,PT}$ , in which  $g_p/2 = 2.7928473441$  is used<sup>8</sup>. Next, we move the cyclotron particle to the PKT centre and the Larmor particle from the AT to the PT, by applying voltage ramps to the transport electrodes that interconnect the traps. Then a spin-flip drive at  $v_{rf,PT}$  is irradiated for a time t<sub>SE,PT</sub>, transmitted by a coil mounted close to the PT (Fig. 1a). Afterwards, we move the Larmor particle back to the AT and the cyclotron particle to the PT and cool its magnetron mode. To identify whether the spin in the PT was flipped, we record a subsequent  $v_{z,AT}$ /spin flip sequence to compare the spin state in which the particle was leaving the AT and once it returns from the PT. Here we identify a measured  $v_z$ jump of  $\Delta v_z > \Delta v_{z,SF}/2 = 0.173/2$  Hz as a detected spin transition<sup>21</sup>. The error rate of identifying the spin flips driven in the PT depends on the axial frequency scatter of the  $v_{z,AT}$  sequences; the formalism to correctly estimate the error rate is described in refs. 30,31. The median

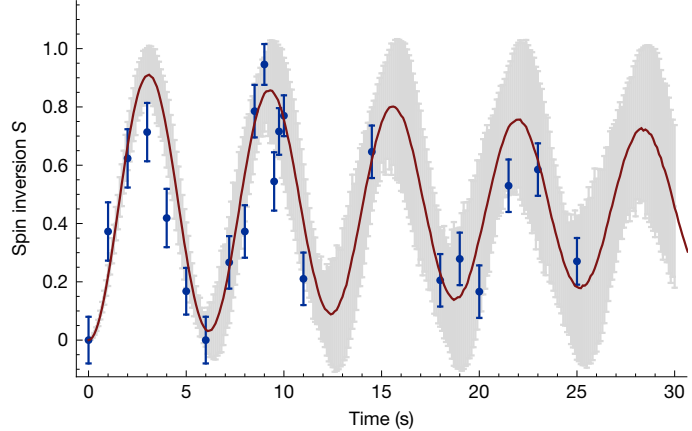


**Fig. 3** | **Antiproton Rabi oscillations.** Observation of coherent Rabi oscillations of the spin of a single trapped antiproton. The blue points represent the measured data and the red line depicts a Monte Carlo fit, which assumes  $52 \, \text{mHz}$  cyclotron frequency measurement decoherence as determined in the related measurements. In grey are the uncertainties of the Monte Carlo simulation. The effective coherence time is  $\tau_{s,p\tau} = 50.2(4)$  s. Each point is an average of 20 spin flip attempts, uncertainty bars represent the standard deviations of the measured data distributions. Throughout the measurement campaign we have recorded several of these plots for different Rabi frequencies.

axial frequency scatter of 32(2) mHz corresponds to an error rate less than 5%.

By applying this protocol and adjusting the radiofrequency interrogation time  $t_{\rm SF,PT}$  to drive spin transitions in the PT, we repeat the procedure 20 times for each value of  $t_{\rm SF,PT}$ , thereby obtaining the spin-flip probability  $P(t_{\rm SF,PT})$ , shown as the blue data points in Fig. 3. This corresponds to the first observation of Rabi oscillations with a single nuclear spin 1/2 antiparticle. The red line is a Monte Carlo fit (Methods and Extended Data Table 3) of

$$L(\Omega_0, \Delta, t) = \int_{-\infty}^{\infty} P_{\mathsf{SF},\mathsf{PT}}(\Omega_0, \Delta + \sigma, t) \, G(\sigma; \mu, \sigma) \, \mathrm{d}\sigma,$$

in which the function

$$P_{\text{SF,PT}}(\Omega_0, \Delta, t) = \frac{\Omega_0^2}{\Omega_0^2 + \Delta^2} \times \sin^2\left(\pi\sqrt{\Omega_0^2 + \Delta^2} \times t\right),$$

is the spin-flip probability with Rabi frequency  $\Omega_0$ , detuning  $\Delta = \nu_{rf,PT} - \nu_L$  and interrogation time t. The function  $G(\mu,\sigma)$  is a Gaussian distribution, defined by the scatter  $\sigma \approx 52$  mHz, arising from the  $\nu_{c,PT}$  measurement noise present during these experiments. This noise leads to an observed decay of spin inversion, to which an effective spin coherence time of  $\tau_{s,PT} = 50.2(4.8)$  s can be assigned. For further details on the analysis, see Methods. This indicates that, in an optimized Rabi resonance scan, executed on the  $\pi$ -pulse, a FWHM  $\Delta\nu_{FWHM} \approx 20$  mHz or 250 ppt could be achieved. We note that magnetic noise imposed by the accelerator reduces the spin coherence time to 5.6(4) s (Extended Data Fig. 1).

To optimize the spectral response of the coherent dynamics for measurements at optimum line-centre resolution, we first record Rabi oscillations at different drive amplitudes and determine the  $t_{\text{SF,PT}}$  in the PT at which maximum inversion is achieved. At the determined optimum  $t_{\text{SF,PT}}$ , we perform Larmor resonance scans, keeping  $t_{\text{SF,PT}}$  constant while scanning the frequency  $v_{\text{rf,PT}}$  of the spin-flip drive with respect to  $v_{\text{L}} = (g/2) \times v_{\text{c,PT}}$ . Here  $v_{\text{c,PT}}$  is obtained with the cyclotron particle in the PT, extracted from a sequence of six frequency measurements, taken before the application of the spin-flip drive. To resolve the resonance, we sample ten points per irradiated  $v_{\text{rf,PT}}$  and scan each resonance with

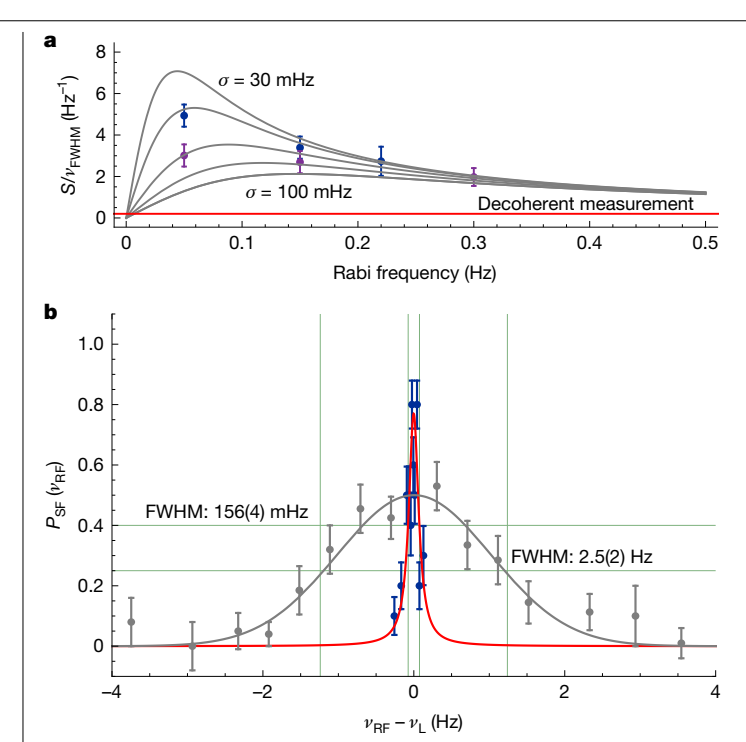


**Fig. 4** | **Antiproton spin resonance. a**, Signal  $S/\Delta v_{\text{FWHM}}$  for different Rabi frequencies and  $\sigma_{c,PT}$ . The grey lines are calculated results for  $\sigma_{c,PT} = 30,40,60,80$ and 100 mHz. **b**, Measured coherent  $v_i$  resonance at the optimized parameters  $found in the \, experiment, \, blue \, scatters \, and \, best \, least-squares \, fit \, of \, a \, Voigt \, profile \, and \, best \, least-squares \, fit \, of \, a \, Voigt \, profile \, and \, best \, least-squares \, fit \, of \, a \, Voigt \, profile \, and \, best \, least-squares \, fit \, of \, a \, Voigt \, profile \, and \, best \, least-squares \, fit \, of \, a \, Voigt \, profile \, and \, best \, least-squares \, fit \, of \, a \, Voigt \, profile \, and \, best \, least-squares \, fit \, of \, a \, Voigt \, profile \, and \, best \, least-squares \, fit \, of \, a \, Voigt \, profile \, and \, best \, least-squares \, fit \, of \, a \, Voigt \, profile \, and \, best \, least-squares \, fit \, of \, a \, Voigt \, profile \, and \, best \, least-squares \, fit \, of \, a \, Voigt \, profile \, and \, best \, least-squares \, fit \, of \, a \, Voigt \, profile \, and \, best \, least-squares \, fit \, of \, a \, Voigt \, profile \, and \, best \, least-squares \, fit \, of \, a \, Voigt \, profile \, and \, best \, bes$ to the data (solid red line). The grey data points are from the previously measured antiprotong-factor resonance8. The coherent line has 1.54 times higher signalto-noise ratio and a FWHM (green vertical lines) that is about 16 times narrower than the width in ref. 8. For both plots, the uncertainty bars represent the standard deviations of the measured data distributions.

a minimum amount of eight discrete frequency offsets, which typically takes 60 h. The recorded cyclotron frequency sequence allows us to study  $\Delta v_{\text{FWHM}}$  and the inversion S as a function of  $v_{\text{c,PT}}$  averages used to reconstruct  $v_1$  at the time when the spin-flip drive is applied in the PT. Averaging several magnetic field measurements for the v<sub>1</sub> reconstruction decreases the cyclotron frequency scatter  $\sigma_{c,PT}$  to about 30 mHz, which narrows the width of the Larmor resonance while increasing the inversion. This is shown in Fig. 4a, in which we plot the ratio of inversion  $S \in [0, 1]$  over the measured  $\Delta v_{\text{FWHM}}$  as a function of the Rabi frequency  $\Omega_0/(2\pi)$  applied to sampled spin resonances. The purple data points are for one  $v_{c.PT}$  measurement and the blue points are for four averages that are used to extrapolate  $v_i$ . The grey lines represent the calculated scalings for different cyclotron frequency fluctuations between  $\sigma = 30$ and 100 mHz. More than four  $v_{c,PT}$  averages, due to a random walk in the field of the superconducting magnet, adds further fluctuation, broadening the Larmor resonance line again.

By systematically scanning the interrogation times and Rabi frequencies, we obtain at  $\Omega_0/(2\pi) \approx 50$  mHz and a drive time of 16 s a signal inversion of 0.77(4) at  $\Delta v_{\text{FWHM}} = 156(4)$  mHz, as shown in Fig. 4b. The blue data points represent the measurement described here and the red line is a fit of a Voigt profile. Compared with the previous most precise measurement of the antiproton magnetic moment8 (grey data in Fig. 4b), this corresponds to an increase of the inversion by a factor of 1.54 at a 16-fold reduction of the FWHM of the resonance line. The line-centre determination of the dataset is at a level of 12 mHz or 150 ppt statistical uncertainty, ten times more accurate than in ref. 8. Note that this resonance was sampled during a data-taking period of only about 60 h, whereas the data accumulation in our previous measurement took place over a period of two months.

The statistical uncertainty in determining the line centre of such g-factor resonances scales proportionally to  $\Delta v_{\text{FWHM}}/S$ . Consequently, on the basis of our coherent spin spectroscopy data, we infer that, under present experimental conditions—relative to those reported in ref. 8-an approximately 25-fold improvement in the statistical precision of the g-factor line-centre determination is achievable. However, the two-particle method introduces systematic limitations on the interpretation of the measured line centre. Specifically, the transfer of particles between the AT and the PT induces magnetic field variations and voltage settling drifts. These effects undermine the critical assumption that the magnetic field remains constant between the  $v_{c,pT}$ measurements and the application of the Larmor drive—a requirement for the precise determination of the antiproton magnetic moment. Quantifying the complete systematic uncertainty budget within the limited three-month annual shutdown of the accelerator remains a substantial challenge. Because accelerator operation reduces the spin coherence time by nearly an order of magnitude, systematic shifts during on and off periods differ. Although using a single-particle doubletrap technique<sup>21</sup> could mitigate the present systematic uncertainties, this approach would substantially extend the required data acquisition time-beyond what is feasible during the short shutdown windows. To address these limitations, we have developed the transportable antiproton trap BASE-STEP<sup>32</sup>, enabling the relocation of antiprotons to dedicated, quiet laboratory environments at HHU Düsseldorf and CERN. These facilities will host precision experiments not exposed to accelerator-induced magnetic field fluctuations. By combining coherent spin quantum spectroscopy with phase-coherent cyclotron frequency measurements in such an environment, it will become feasible to suppress magnetic field noise by at least a factor of five. This would allow statistical resolutions of the g-factor line centre at the level of approximately 10 ppt. The application of these techniques to the proton would open the path towards one of the most stringent tests of CPT invariance in the baryon sector<sup>12</sup>.

#### **Online content**

Any methods, additional references, Nature Portfolio reporting summaries, source data, extended data, supplementary information, acknowledgements, peer review information; details of author contributions and competing interests; and statements of data and code availability are available at https://doi.org/10.1038/s41586-025-09323-1.

- Ludlow, A. D., Boyd, M. M., Ye, J., Peik, E. & Schmidt, P. O. Optical atomic clocks. Rev. Mod. Phys. 87, 637-701 (2015).
- Benhelm, J., Kirchmair, G., Roos, C. & Blatt, R. Experimental quantum-information processing with <sup>43</sup>Ca<sup>+</sup> ions. Phys. Rev. A 77, 062306 (2008).
- Heil, W. et al. Spin clocks: probing fundamental symmetries in nature. Ann. Phys. 525, 539-549 (2013).
- Safronova, M. et al. Search for new physics with atoms and molecules. Rev. Mod. Phys. 90, 025008 (2018).
- Kellogg, J. M. B., Rabi, I. I., Ramsey, N. F. Jr & Zacharias, J. R. The magnetic moments of the proton and the deuteron. The radiofrequency spectrum of H<sub>2</sub> in various magnetic fields. Phys. Rev. 56, 728 (1939).
- Ramsey, N. F. et al. Experiments with separated oscillatory fields and hydrogen masers. Rev. Mod. Phys. 62, 541 (1990)
- Abel, C. et al. Measurement of the permanent electric dipole moment of the neutron. Phys. Rev. Lett. 124, 081803 (2020).
- Smorra, C. et al. A parts-per-billion measurement of the antiproton magnetic moment. Nature 550, 371-374 (2017).
- Borchert, M. et al. Measurement of ultralow heating rates of a single antiproton in a cryogenic Penning trap. Phys. Rev. Lett. 122, 043201 (2019).
- Ulmer, S. et al. Observation of spin flips with a single trapped proton. Phys. Rev. Lett. 106, 253001 (2011)
- Allmendinger, F. et al. New limit on Lorentz-invariance- and CPT-violating neutron spin interactions using a free-spin-precession <sup>3</sup>He-<sup>129</sup>Xe comagnetometer. Phys. Rev. Lett. 112,
- Kostelecky, V. A. & Russell, N. Data tables for Lorentz and CPT violation. Rev. Mod. Phys.
- Fan, X., Myers, T. G., Sukra, B. A. D. & Gabrielse, G. Measurement of the electron magnetic moment. Phys. Rev. Lett. 130, 071801 (2023).
- Fan, X. et al. One-electron quantum cyclotron as a milli-eV dark-photon detector. Phys. Rev. Lett. 129, 261801 (2022).

- Schneider, A. et al. Direct measurement of the <sup>3</sup>He<sup>+</sup> magnetic moments. Nature 606, 878-883 (2022)
- Dickopf, S. et al. Precision spectroscopy on <sup>9</sup>Be overcomes limitations from nuclear structure. Nature 632, 757-761 (2024).
- Smorra, C. et al. BASE-the Baryon Antibaryon Symmetry Experiment. Eur. Phys. J. Spec. Top. 224, 3055-3108 (2015).
- Schneider, G. et al. Double-trap measurement of the proton magnetic moment at 0.3 parts per billion precision. Science 358, 1081-1084 (2017).
- Dehmelt, H. Continuous Stern-Gerlach effect: principle and idealized apparatus. Proc. Natl Acad. Sci. USA 83, 2291-2294 (1986).
- Dehmelt, H. Continuous Stern-Gerlach effect: noise and the measurement process. Proc. Natl Acad. Sci. USA 83, 3074-3077 (1986).
- Mooser, A. et al. Direct high-precision measurement of the magnetic moment of the proton. 21. Nature 509, 596-599 (2014).
- Latacz, B. M. et al. Orders of magnitude improved cyclotron-mode cooling for nondestructive spin quantum transition spectroscopy with single trapped antiprotons. Phys. Rev. Lett. 133, 053201 (2024).
- Smorra, C. et al. Direct limits on the interaction of antiprotons with axion-like dark matter. Nature 575, 310-314 (2019)
- Sellner, S. et al. Improved limit on the directly measured antiproton lifetime. New J. Phys. 19, 083023 (2017).
- 25. Gabrielse, G., Haarsma, L., & Rolston, S. Open-endcap Penning traps for high precision experiments. Int. J. Mass Spectrom. Ion Process. 88, 319-332 (1989).
- Gabrielse, G., & Tan, J. Self-shielding superconducting solenoid systems. J. Appl. Phys. 63, 5143-5148 (1988).
- Devlin, J. A. et al. Superconducting solenoid system with adjustable shielding factor for precision measurements of the properties of the antiproton. Phys. Rev. Appl. 12, 044012

- Brown, L. S. & Gabrielse, G. Geonium theory: physics of a single electron or ion in a Penning trap. Rev. Mod. Phys. 58, 233 (1986)
- Borchert, M. et al. A 16-parts-per-trillion measurement of the antiproton-to-proton charge-mass ratio. Nature 601, 53-57 (2022).
- Smorra, C. et al. Observation of individual spin quantum transitions of a single antiproton. Phys. Lett. B 769, 1-6 (2017).
- Mooser, D. et al. Resolution of single spin flips of a single proton. Phys. Rev. Lett. 110, 140405 (2013).
- 32. Smorra, C. et al. BASE-STEP: a transportable antiproton reservoir for fundamental interaction studies. Rev. Sci. Instrum. 94, 113201 (2023).

Publisher's note Springer Nature remains neutral with regard to jurisdictional claims in published maps and institutional affiliations.



Open Access This article is licensed under a Creative Commons Attribution-NonCommercial-NoDerivatives 4.0 International License, which permits any non-commercial use, sharing, distribution and reproduction in any medium or

format, as long as you give appropriate credit to the original author(s) and the source, provide a link to the Creative Commons licence, and indicate if you modified the licensed material. You do not have permission under this licence to share adapted material derived from this article or parts of it. The images or other third party material in this article are included in the article's Creative Commons licence, unless indicated otherwise in a credit line to the material. If material is not included in the article's Creative Commons licence and your intended use is not permitted by statutory regulation or exceeds the permitted use, you will need to obtain permission directly from the copyright holder. To view a copy of this licence, visit http:// creativecommons.org/licenses/by-nc-nd/4.0/.

© The Author(s) 2025

## Methods

#### Penning-trap frequencies

A Penning trap is a superposition of a strong magnetic field, for BASE  $B_0 = 1.945$  T and electrostatic potential  $\phi = V_0 C_2 (z^2 - \rho^2/2)$ . Here z and  $\rho$  are cylindrical coordinates, the z-axis is defined by the magnetic field axis and z = 0 is the centre of the central ring electrode of the trap. The voltage  $V_0$  is applied to the central ring electrode of the five-electrode traps<sup>25</sup> used and  $C_2$  is a trap-specific geometry coefficient, related to the size of the trap electrodes. In magnetic field  $B_0$ , a particle of charge q and mass m is oscillating at the free cyclotron frequency

$$v_{\rm c} = \frac{1}{2\pi} \frac{q}{m} B$$
.

The electrostatic potential confines the particle in the axial direction, leading to an axial oscillation along the magnetic field lines at

$$v_z = \frac{1}{2\pi} \sqrt{\frac{2qC_2V_0}{m}}.$$

The potential also modifies the cyclotron frequency to the modified cyclotron frequency  $\nu_+$ . Also, the crossed magnetic and electric field leads to a slow drift at the magnetron frequency  $\nu_-$ , both modes oscillating perpendicular to the magnetic field lines at

$$v_{+} = \frac{1}{2} \left( v_{c} + \sqrt{v_{c}^{2} - 2v_{z}^{2}} \right)$$

and

$$v_{-} = \frac{1}{2} \left( v_{c} - \sqrt{v_{c}^{2} - 2v_{z}^{2}} \right).$$

The most relevant parameters of the AT and the PT are summarized in Extended Data Table 1.

#### **Image current detectors**

The particle frequencies  $v_+$ ,  $v_z$  and  $v_-$  are measured by image current detection<sup>33</sup>. A schematic illustrating the working principle of such a detector is shown in Fig. 1b. The concept is that a superconducting inductor L is connected to one of the trap electrodes. Together with the capacitance  $C_p$  of the trap, it forms a parallel tuned circuit that acts at its resonance frequency  $v_r$  as an effective parallel resistance  $R_p = 2\pi v_r Q L$ , in which Q is the quality factor of the tuned circuit. The particle-induced image current (for example, axial oscillation)

$$i_{\rm p} = \frac{q}{D_{z}} (2\pi v_{z,\rm p}) z$$

then induces a voltage drop

$$u_p = R_p \times i_p = R_p \times \frac{q}{D_z} (2\pi v_{z,p}) z.$$

Here the parameter  $D \approx 0.01$  m is the effective electrode distance, which depends on the trap geometry and the distance to the pickup electrode to which the detector is connected (Extended Data Table 2).

**Sensitivity.** For the detector resistances of typically  $R_{\rm p}\approx 100~{\rm M}\Omega$  and the thermal noise of  $e_{\rm n}\approx \sqrt{4k_{\rm B}T_zR_{\rm p}}$ , the top noise level of the detector at its resonance frequency  $v_{\rm r}$ , it is possible to detect a particle at an oscillation amplitude of about 100  $\mu$ m, inducing an image current of about 10 fA.

Owing to the particle–detector interaction, once the particle frequency  $\nu_{z,p}$  is tuned to  $\nu_r$ , excited particles are damped with a cooling time constant

$$\tau_{\rm p} = \frac{m}{2\pi v_{\rm r} QL} \frac{D^2}{q^2} \,.$$

A particle in thermal equilibrium with the detector shorts the detector's thermal Johnson noise and appears as a dip at its axial frequency  $v_z$  on the measured noise spectrum?9. The FWHM of the dip is proportional to the damping  $\Delta v_z = 1/(2\pi r_p)$ . This 'dip detection' technique—in which we determine  $v_z$  by fitting a function to the measured detector noise spectra—is used for the axial frequency measurements in the AT as well as for the cyclotron frequency measurements in the PT, as discussed in detail in ref. 29.

#### Recent experiment upgrades

In comparison with our previous measurement of the antiproton magnetic moment<sup>30</sup>, the experimental set-up has undergone a comprehensive upgrade, resulting in notable performance gains. Key enhancements include a complete overhaul of the cryogenic electronics: the cyclotron and axial detection systems have been improved, the frequency tuning range of the cyclotron detectors has been extended and the cryogenic filtering and switching stages have been optimized. Moreover, the implementation of a dedicated cooling trap<sup>22</sup> has led to a substantial increase of cold-particle preparation time.

Further stability has been achieved by reengineering the cryogenic trap inlay and integrating a magnetic tuning and self-shielding system, ensuring precise magnetic field control and long-term operational reliability. Together, these developments enable higher experimental throughput, faster particle preparation and faster and more robust data acquisition.

These technical advancements directly translate into improved control over the spin degree of freedom. Spin-state initialization now reaches fidelities of  $F \approx 100\%$ , whereas quantum projection measurements of spin flips in the PT consistently achieve fidelities exceeding 95% (ref. 22).

# Simulated likelihood estimation of Rabi oscillations

When applying a spin-flip drive in the PT, we define the frequency  $v_{rf}$ to drive the spin transitions based on the cyclotron frequency measurements executed with the cyclotron particle in the PT. The used double-dip frequency measurement method, explained in detail in ref. 29, has an intrinsic frequency fluctuation  $\sigma_{c,PT}(t)$  that depends on the frequency measurement time. For short frequency averaging time, the fluctuation of the determined  $v_{c,PT}$  is dominated by thermalnoise fluctuations of the frequency spectrum; for very long frequency averaging times, the magnetic field of our superconducting magnet is drifting away. At the optimum frequency averaging time of about 540 s, we obtain a frequency fluctuation of  $\sigma_{c,PT}(t)/v_{c,PT} \approx 800$  ppt. To understand our data, which evolve under both deterministic laws and random influences, we use Monte Carlo simulations and model the experiment protocol described in the main text, in which we execute for one particular interrogation time  $t_{SE,PT}$  a total of 20 spinflip experiments at drive frequency  $v_{rf}$  that is defined by  $(g_{\overline{p}}/2) \times v_{c,PT}$ . Note that the fluctuation  $\sigma_{c,PT}$  limits our ability to irradiate the exact on-resonant  $v_{rf} = v_L$ , which effectively leads to a convolution of the time-dependent spin dynamics  $P_{\text{SEPT}}(\Omega_0, \Delta, t)$  given in the main manuscript with the frequency measurement fluctuation  $\sigma_{\rm c,PT}$  . Our measured results are mean values of  $P_{SF,PT}(\Omega_0, \Delta, t)$  for different values of the detuning parameter  $\Delta$  that is noised by the measurement fluctuation  $\sigma_{c.PT}$ .

To evaluate the data, we use a simulated maximum likelihood method. We first simulate the influence of measurement noise using a Mersenne Twister pseudo-random number generator to model the distribution of  $\sigma_{c,PT}$  fluctuations. These are used to generate a set of randomly detuned spin-flip responses  $P_{SE,PT}(\Omega_0, \Delta, t)$ , whose averages

are calculated. We estimate the likelihood L of the data by averaging over the simulated likelihoods and applying a Nelder–Mead algorithm to maximize it to find the best-fit parameters. The confidence intervals on the fit parameters  $\theta_k$  are obtained by evaluating  $l(\theta) = \log(L(\theta))$  and numerically solving  $-2(l(\theta) - l(\hat{\theta})) = 1$ , in which  $\hat{\theta}$  is the parameter value that maximizes the likelihood. The red line in Fig. 3 represents the optimized average result obtained by this algorithm and the grey-shaded area represents the results of 10,000 simulations for different random detuning parameters  $\Delta$ .

Finally, the effective spin coherence time is extracted by fitting an exponentially damped oscillator to the average outcome of the Monte Carlo simulations optimized through this likelihood analysis. The results of the best fit are summarized in Extended Data Table 3.

#### Rabi oscillations with the accelerator on

The experiments were conducted in the AD/ELENA antimatter facility of CERN. The magnetic ramps of the antiproton decelerator magnets running in the background induce magnetic field fluctuations with amplitudes on the 1.6  $\mu T$  level, which reduce the spin coherence time to 5.4(6) s, as shown in Extended Data Fig. 1.

## **Ethics Statement**

Our work values diverse perspectives, promotes diversity and upholds the highest standards of integrity in research and communication. We strive to ensure that science serves the global community responsibly.

#### **Data availability**

All data presented in the manuscript will be made available on request to the corresponding author.

## **Code availability**

All code used for data evaluation will be made available on request to the corresponding author.

 Wineland, D., & Dehmelt, H. Principles of the stored ion calorimeter. J. Appl. Phys. 46, 919–930 (1975).

Acknowledgements We acknowledge technical support by CERN, especially the Antiproton Decelerator operation group, CERN's Cryolab team and Engineering Department and all of the other CERN groups that provide support to Antiproton Decelerator experiments. We acknowledge financial support by HHU Düsseldorf, RIKEN, the Max Planck Society, CERN, the European Union, the Helmholtz-Gemeinschaft and the Max Planck-RIKEN-PTB Center for Time, Constants and Fundamental Symmetries.

Author contributions The experiment was designed and built by S.U., C.S. and B.M.L. Several important technical upgrades were developed and implemented by M.F., S.R.E., P.G., J.I.J., P.M. and J.A.D. S.U., B.M.L., S.R.E., M.F., E.W., J.I.J. and J.A.D. developed and commissioned the experiment control code. S.U. developed the strategy of coherent antiproton spin spectroscopy that was implemented by S.U. and B.M.L., supported by new instrumentation developed by S.R.E. and M.F. B.M.L., S.U. and J.I.J. took part in experiment commissioning and the data acquisition. B.M.L., S.U., J.I.J., E.W., T.I. and B.P.A. contributed to the maintenance of the experiment during the measurement campaign. The data were analysed by S.U. and B.M.L. and discussed with A.M., K.B., C.S., A.S. and C.O. during analysis and with F.A., M.L., D.S., F.V. and H.Y. during group meetings. S.U., K.B., C.O., C.S., B.M.L., Y.M., W.Q., A.S., J.W. and Y.Y. contributed to the financing and supervision of staff who operate and maintain the experiment and who conducted the measurements. The manuscript was written by S.U. and B.M.L. and revised by K.B., C.S., J.A.D. and A.M. All co-authors discussed, iterated, improved and approved the content.

Competing interests The authors declare no competing interests.

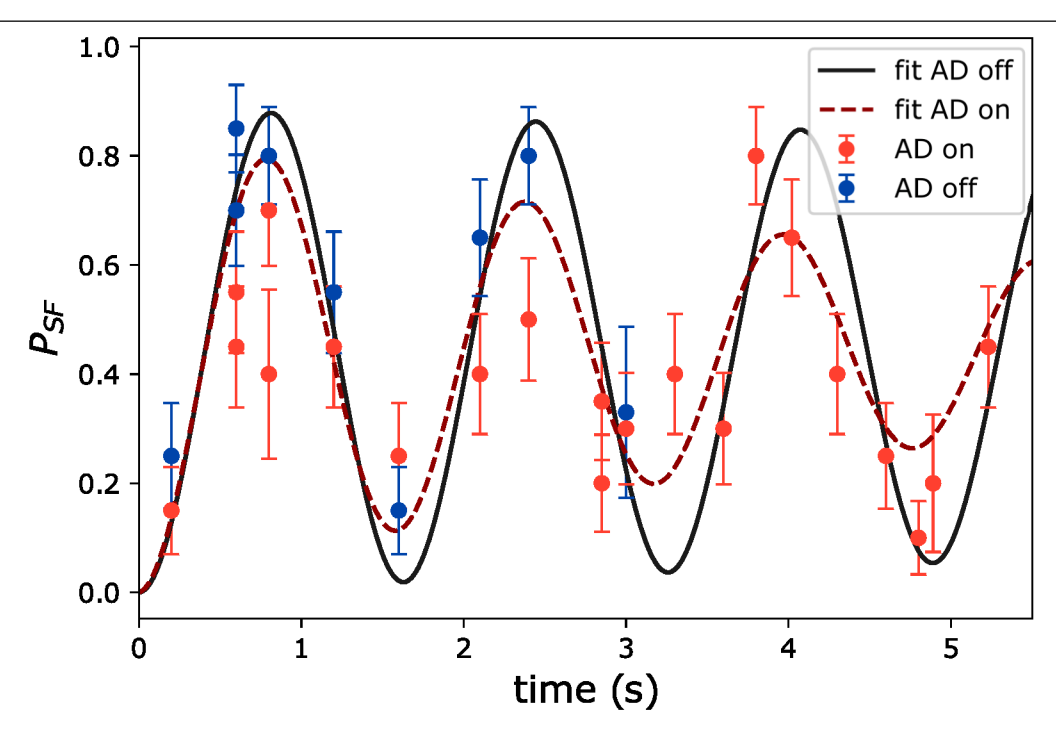
#### Additional information

Supplementary information The online version contains supplementary material available at https://doi.org/10.1038/s41586-025-09323-1.

Correspondence and requests for materials should be addressed to S. Ulmer.

Peer review information Nature thanks Jens Dilling, Jeffrey Hangst and the other, anonymous, reviewer(s) for their contribution to the peer review of this work. Peer reviewer reports are available.

Reprints and permissions information is available at http://www.nature.com/reprints.



**Extended Data Fig. 1** | **Rabi oscillations 'accelerator on'.** Spin coherence during accelerator uptime. The magnetic field ramps of the accelerator reduce the antiproton spin coherence time to about 5.4(6) s. Data represent mean

values of at least 10 attempts per individual setting, uncertainty bars are the standard deviations of the individual data sets.

# Extended Data Table 1 | Trap parameters for the PT and AT

Quantity	PT	AT
$B_0$	1.945T	1.212T
<b>V</b> <sub>0</sub>	4.572V	0.855V
<i>C</i> <sub>2</sub>	18500/m <sup>2</sup>	114000/m <sup>2</sup>
V <sub>L</sub>	82.813MHz	51.651MHz
V <sub>C</sub>	29.652MHz	18.494MHz
V <sub>+</sub>	29.646MHz	18.482MHz
V <sub>z</sub>	637kHz	658kHz
V_	7kHz	12kHz

# Extended Data Table 2 $\mid$ Axial detector parameters for the PT and AT

Quantity	PT	AT
Pickup	Correction	Endcap
	Electrode	Electrode
Q	10400	24600
L	1.71mH	2.19mH
V <sub>Z</sub>	637kHz	658kHz
$R_{\rho}$	71ΜΩ	223ΜΩ
D	10.0 mm	11.2mm
Tp	0.092s	0.037s
$\Delta v_z$	1.7Hz	4.3Hz
$T_z$	8.5K	14.7K

Extended Data Table 3 | Fit parameters of the simulated maximum likelihood estimate. C.L. of the fit parameter as defined in the text

Quantity	Parameter	C.L. (0.68)
Inversion S	0.89	0.11
Rabi Frequency $\Omega_0$	0.155Hz	0.003Hz
Coherence time $ au_{s,PT}$	50.2s	4.8s